

Joint spectral and polarimetric analysis of hot star wind transients

This article has been downloaded from IOPscience. Please scroll down to see the full text article.

1995 Inverse Problems 11 79

(<http://iopscience.iop.org/0266-5611/11/1/005>)

[The Table of Contents](#) and [more related content](#) is available

Download details:

IP Address: 130.251.61.251

The article was downloaded on 13/10/2009 at 13:44

Please note that [terms and conditions apply](#).

Joint spectral and polarimetric analysis of hot star wind transients

P Calvini[†], M Bertero[†] and J C Brown[‡]

[†] Istituto Nazionale di Fisica Nucleare and Dipartimento di Fisica dell'Università di Genova, via Dodecaneso 33, I-16146 Genova, Italy

[‡] Department of Physics and Astronomy, University of Glasgow, Glasgow G12 8QQ, UK

Received 18 July 1994

Abstract. The problem of deriving the evolution of stellar mass loss rate $m(\tau)$ and asphericity $a(\tau)$ from data on episodic polarization and absorption line strength variations is considered following the treatment by Brown and Wood. Their method, based on Fourier solution of a pair of coupled convolution equations, is tested on simulated data from a variety of hypothetical models for $m(\tau)$ and $a(\tau)$. Moreover, we investigate a new method which requires fewer data points than Fourier deconvolution and can be readily extended to the case of non-uniformly spaced and non-simultaneous (though overlapping) data for polarization and absorption measurements. This method provides a regularized solution in a space of differentiable functions (Sobolev space) and in our tests it proves to be as reliable as Fourier deconvolution. Moreover, various criteria for the choice of the regularization parameters are compared in view of the application to the analysis of real data. Both the methods considered are reliable for the estimation of $m(\tau)$ and $a(\tau)$ in the presence of realistic data noise.

1. Introduction

Loss of mass from their outer layers is a phenomenon exhibited by most stars to a greater or lesser extent. Some of these stellar winds are very weak. That of the sun, for example, is driven by the gas pressure of the hot outer layers (corona) as predicted by Parker [1], was suggested earlier by Bierman [2] because of the behaviour of comet tails, and has been detected directly by spacecraft [3]. The solar wind would take over 10^{14} years to remove all of the sun's mass—about 10^5 times the sun's age [4]. Others are very powerful, driven primarily by the high radiation pressure of hot stars, removing stellar matter at rates up to a solar mass in 10^4 years—see, e.g. reviews [5, 6]. The simple steady spherically symmetric structure, which might be expected for such winds on the basis of simple stellar models, is in practice greatly complicated by little understood physical processes, which cause the wind to be highly aspherical and to exhibit transient mass loss rate variations (mass loss episodes). Among the factors influencing such behaviour are the centrifugal force of stellar rotation, changes in stellar shape due to non-radial pulsation, localized surface magnetic fields and radiative/hydrodynamic instabilities [7]. Since the theoretical physics underlying these effects is so poorly understood, it is particularly important to develop diagnostic methods for analysis of data which reflect the behaviour of the wind material.

There are many indicators of the density n , temperature T and velocity v field distribution of matter in the wind volume V around such stars. Since most winds are not spatially resolved, all of these indicators are integrals over the wind volume and therefore the spatial structure can only be inferred via its deconvolution from observed photon properties

through reasonable models of the radiation process involved. Among these indicators are: (a) the strengths of collisionally excited emission lines or of continuum radiation from the whole wind volume V (these depend on $\int_V n^2 \Phi(T) dV$ where $n(r)$ and $T(r)$ are the local electron density and temperature at r and $\Phi(T)$ depends on atomic rate coefficients); (b) the strengths of absorption lines formed along the line of sight s to the stellar disk (these depend on $\int_s n \Psi(n, T) ds$ where Ψ depends on atomic absorption and collision rate coefficients); (c) the broad-band polarization of electron scattered starlight, which depends on $\int_V n S dV$ where the weight $S(r)$ comes from the Thomson scattering matrix [8]; (d) the spectropolarimetric line profiles of stellar spectrum lines, which depend on the n and v distributions over V [9, 10]. Of these only the polarimetric data carry information on the angular distribution of the wind. Brown and Henrichs [11], following data from Sonneborn *et al* [12], first pointed out that by combined analysis of data on absorption line strength and polarization it should be possible to separate the evolution of mass loss rate and shape (asphericity) in a mass loss episode. This was confirmed by the analysis of Brown and Wood [13] who, under certain simplifying assumptions, reduced the problem to the solution of a pair of separable linear convolution equations. In their analysis Brown and Wood demonstrated the feasibility of the deconvolution, but examined only the most obvious Fourier method. They did not consider the question of optimal methods for obtaining a regularized solution for non-uniformly spaced data or in the presence of data noise. In the present paper we re-examine the problem from this viewpoint and consider synthetic data from a number of hypothetical models of the mass loss rate and shape evolution. These are chosen to test the recoverability of features of particular interest such as pulsation in the mass loss function indicative of the influence of stellar pulsation on the mass loss process. The effects of gaps in the data will be examined in a future publication as well as the application to real data.

The basic equations in dimensionless form, as derived in [13], are the following

$$F(\tau) = \int_{-\infty}^{\tau} m(\tau') a(\tau') \frac{\sqrt{(\tau - \tau')(\tau - \tau' + 2)}}{(\tau - \tau' + 1)^3} d\tau' \quad (1.1)$$

$$G(\tau) = \int_{-\infty}^{\tau} m(\tau') [1 - a(\tau') \cos^{\delta} i] \frac{d\tau'}{(\tau - \tau' + 1)^2}. \quad (1.2)$$

Here $F(\tau)$ and $G(\tau)$ are functions proportional, respectively, to the degree of polarization and the absorption line strength; $m(\tau')$ is proportional to the equatorial mass loss $\dot{M}_0(t)$ and $a(\tau')$ is related to the envelope shape function $S(t)$ (in effect $1 - a$ is equal to the ratio of polar to equatorial mass loss rates); the variables τ and τ' are dimensionless times measured in units of $t_0 = R/v_0$ where R is the stellar radius and v_0 is the flow speed (taken as constant) in the radial direction and i is the inclination to the observer of the axially symmetric envelope.

Equations (1.1) and (1.2) form a pair of nonlinear coupled equations for the unknown functions $m(\tau')$ and $a(\tau')$. The nonlinearity, however, is rather simple and therefore, as suggested in [13], one can try to solve the two equations separately and recover functions which are simply related to $m(\tau')$ and $a(\tau')$. In this paper we will use this approach.

In section 2 we consider the regularized solution of (1.1) and (1.2) by using the Fourier transform. This method can be used if the functions $F(\tau)$ and $G(\tau)$ are uniformly sampled at the correct rate on the observation time interval, which, in general, must be longer than the duration of the episodic mass loss. Since this condition is never satisfied in practice, one must consider the case where the functions $F(\tau)$ and $G(\tau)$ are given only at a general finite

set of points τ_i to which the Fourier method cannot be applied. This problem is formulated in section 3 for uniformly spaced points (non-uniform spacing will be considered in a subsequent paper), assuming that both $m(\tau)$ and $a(\tau)$ belong to a space of differentiable functions (Sobolev space), and its singular value decomposition (SVD) is investigated. In particular, results on the singular value spectrum and on the singular functions are given. In section 4 we apply the results of section 3 to the inversion of simulated data from a number of hypothetical models. Note that we consider the full problem of finding $m(\tau)$ and $a(\tau)$, whereas Brown and Wood [13] consider only the problem of recovering the product $m(\tau)a(\tau)$ (equation (1.1)). The problem of the choice of the regularization parameters is also investigated.

2. Regularized deconvolution using the Fourier transform

If only episodic outbursts are analysed, then, as shown in [13], we can assume $m(\tau') = a(\tau') = 0$ for $\tau' < 0$ and (1.1), (1.2) can be written as follows for $\tau > 0$

$$F(\tau) = \int_0^\tau m(\tau')a(\tau') \frac{\sqrt{(\tau - \tau')(\tau - \tau' + 2)}}{(\tau - \tau' + 1)^3} d\tau' \quad (2.1)$$

$$G(\tau) = \int_0^\tau m(\tau')[1 - a(\tau') \cos^\delta i] \frac{d\tau'}{(\tau - \tau' + 1)^2}. \quad (2.2)$$

Of course, we will also assume that $F(\tau) = G(\tau) = 0$ for $\tau < 0$. Moreover, as suggested in [13], we can introduce the new functions

$$f(\tau) = m(\tau)a(\tau) \quad (2.3)$$

and

$$g(\tau) = m(\tau)[1 - a(\tau) \cos^\delta i]. \quad (2.4)$$

Then, if we denote the kernel functions for $\tau > 0$ as

$$K(\tau) = \frac{\sqrt{\tau(\tau + 2)}}{(\tau + 1)^3} \quad (2.5)$$

and

$$H(\tau) = \frac{1}{(\tau + 1)^2} \quad (2.6)$$

we have the uncoupled equations

$$F(\tau) = \int_0^\tau K(\tau - \tau')f(\tau') d\tau' \quad (2.7)$$

$$G(\tau) = \int_0^\tau H(\tau - \tau')g(\tau') d\tau'. \quad (2.8)$$

Once these have been solved and the functions $f(\tau')$ and $g(\tau')$ have been obtained, the functions $m(\tau')$ and $a(\tau')$ can be derived from

$$m(\tau') = g(\tau') + f(\tau') \cos^{\delta} i \quad (2.9)$$

and

$$a(\tau') = \frac{f(\tau')}{m(\tau')}. \quad (2.10)$$

The difficulties of this procedure are the following: equations (2.7) and (2.8) are ill-posed and therefore, for real data, one must estimate the solution by means of regularization techniques; the estimation of $a(\tau')$ by means of (2.10) can be dangerous, as we shall see, when both $f(\tau')$ and $m(\tau')$ are small (we assume that $m(\tau)$ is normalized in such a way that its maximum value is of the order of one—see the test functions (A.1)–(A.3)).

As concerns (2.7), (2.8), they can be diagonalized by the use of the convolution theorem of the Laplace transform. However, this approach is not convenient because in this way one can estimate the Laplace transform of the solution and one needs, as a final step, the inversion of the Laplace transform, an extremely ill-posed problem. For this reason we use, as in [13], the Fourier transform. For this purpose, all the functions appearing in (2.7), (2.8) must be considered as defined on $(-\infty, +\infty)$, having a value of zero on $(-\infty, 0)$.

By means of this approach, we have investigated the use of Tikhonov regularization in L^2 space (zero-order regularization) [14, 15] for solving (2.7), (2.8). Since the functions $F(\tau)$ and $G(\tau)$ are independent physical quantities which, in general, are affected by different degrees of noise, we must introduce two different regularization parameters, α and β , one for each equation; then the Fourier transforms of the regularized solutions are given by

$$\widehat{f}_{\alpha}(\omega) = \frac{\widehat{K}^*(\omega)}{|\widehat{K}(\omega)|^2 + \alpha} \widehat{F}(\omega) \quad (2.11)$$

$$\widehat{g}_{\beta}(\omega) = \frac{\widehat{H}^*(\omega)}{|\widehat{H}(\omega)|^2 + \beta} \widehat{G}(\omega). \quad (2.12)$$

Once the functions $f(\tau)$ and $g(\tau)$ have been obtained by means of Fourier transform inversion, the function $m(\tau)$ can be derived from (2.9) while the function $a(\tau)$ can be derived from the following regularized version of (2.10)

$$a_{\gamma}(\tau) = \frac{f(\tau)m(\tau)}{[m(\tau)]^2 + \gamma} \quad (2.13)$$

where γ is a further regularization parameter. When m is much greater than $\sqrt{\gamma}$ this equation essentially reduces to (2.10), whereas for m smaller than $\sqrt{\gamma}$ it produces small values of $a(\tau)$. If we look at (2.1) and (2.2), we notice that $a(\tau)$ contributes to $F(\tau)$ and $G(\tau)$ only through the product $m(\tau)a(\tau)$. Therefore the contribution from the time intervals where $m(\tau)$ is small is also small and, in these intervals, it must be difficult to recover the values of $a(\tau)$, without them being dominated by noise. Physically this means that when the current mass loss rate $m(\tau)$ is small, the polarization can only be substantial if it is dominated by large mass loss rates at earlier times, making the current shape of $a(\tau)$ hard to find.

In order to test the recoverability of m and a profiles from F and G data sets in the scheme of FFT inversion when noise is present, we have done some extensive work to create

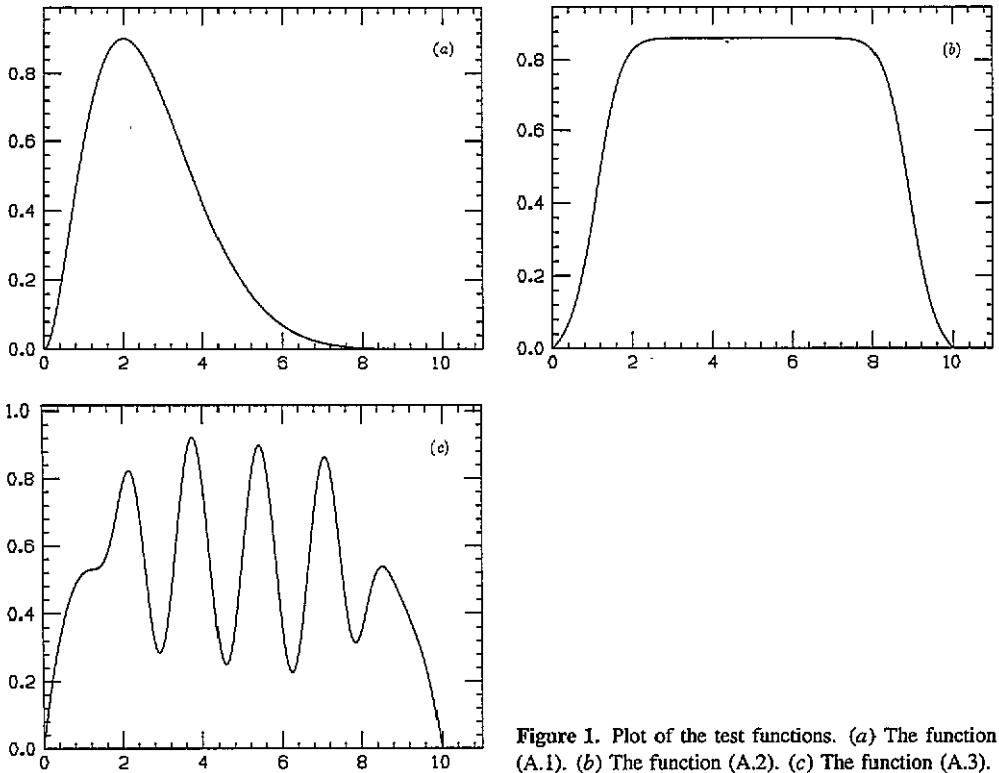


Figure 1. Plot of the test functions. (a) The function (A.1). (b) The function (A.2). (c) The function (A.3).

simulated data and then to estimate the original shapes. We have chosen three test functions, denoted by h_i ($i = 1, 2, 3$), having support on the interval $[0, 10]$ and exhibiting behaviour of potential interest from an astrophysical point of view. Their plots are shown in figure 1 and their mathematical form is presented in appendix A.

In our tests we have considered, in total, nine situations generated by taking as m each one of the h_i functions in turn and doing the same for a , in all possible pairings. In the following we will denote by $\{m_j, a_k\}$ the pair obtained by taking $m(\tau) = h_j(\tau/10)$, $a(\tau) = h_k(\tau/10)$. For reasons concerning point spacings and range in FFT algorithm, the data functions $F(\tau)$ and $G(\tau)$, corresponding to each one of the nine cases, have been computed for 256 values of τ ranging from -20 to 20 (being given by (2.1) and (2.2) in the interval $[0, 20]$ and set to zero in the interval $[-20, 0]$) and using an intermediate value of $\cos^{\delta} i = 0.7$. From now on, we denote noiseless data by \tilde{F} and \tilde{G} and noisy data by F and G . Values of $\tilde{F}(\tau)$ and $\tilde{G}(\tau)$ have been computed from (2.7), (2.8) by means of a numerical integration routine. Noise has been added to the resulting values according to the formulae

$$F(\tau) = \tilde{F}(\tau)(1 + \text{ampl} \cdot \text{rnd}) \quad (2.14)$$

and

$$G(\tau) = \tilde{G}(\tau)(1 + \text{ampl} \cdot \text{rnd}) \quad (2.15)$$

where rnd is a random number having a Gaussian distribution with zero mean and unit variance and ampl was taken as 0.03 (3% Gaussian noise). In this paper we ignore the fact that fractional errors will tend to be larger for smaller data values.

For each $\{m_j, a_k\}$ pairing, we consider 20 realizations of the Gaussian noise in each one of (2.14) and (2.15) in order to produce 20 data sets for $F(\tau)$ and 20 data sets for $G(\tau)$. Then the FFTs of $F(\tau)$, $G(\tau)$ and of the two kernels occurring in (2.1), (2.2) are computed and the FFTs of the regularized solutions $f_\alpha(\tau)$ and $g_\beta(\tau)$ are obtained from (2.11) and (2.12), respectively.

As concerns the choice of the regularization parameters α , β , γ , this always implies a compromise between the approximation error and the effect of noise on the solution. In the case of simulations, it is possible to define an optimum choice by introducing a distance between the regularized solution and the true one and by looking for the value of the parameter minimizing this distance. In this sense we get the best possible approximate solution. Here we proceed as follows.

Consider a pair $\{m, a\}$ with related functions f, g as defined by (2.3) and (2.4). If we denote by τ_i the sampling points of $f(\tau)$ inside some interval of interest (let us say, for instance, the interval $[-5, 11]$), we define the relative RMS error in the estimation of f by means of f_α as

$$\mathcal{E}_f(\alpha) = \frac{\|f - f_\alpha\|_2}{\|f\|_2} \quad (2.16)$$

where the norm is the Euclidean one

$$\|f\|_2 = \left(\sum_i |f(\tau_i)|^2 \right)^{1/2} \quad (2.17)$$

As a function of α , $\mathcal{E}_f(\alpha)$ has a minimum at $\alpha = \alpha_{\text{opt}}$. The corresponding regularized solution $f_\alpha(\tau)$ is the one providing the best approximation of $f(\tau)$ in the sense of RMS errors. In a similar way one defines the relative RMS error in the estimation of $g(\tau)$ by means of $g_\beta(\tau)$, $\mathcal{E}_g(\beta)$, which has a minimum at $\beta = \beta_{\text{opt}}$. When the regularized solutions providing the best approximations of $f(\tau)$ and $g(\tau)$ have been determined, the corresponding approximation of $m(\tau)$ can be obtained from (2.9). The relative RMS error in the estimation of $m(\tau)$ can be computed for each of the twenty noise realizations; the mean value of these 20 relative RMS errors will be denoted by \mathcal{E}_m .

In the case of the function $a(\tau)$, once the best estimates of f, g have been obtained, we have still to choose the regularization parameter γ (see (2.13)). If $\mathcal{E}_a(\gamma)$ is the relative RMS error in the estimation of $a(\tau)$, we can minimize $\mathcal{E}_a(\gamma)$ in order to get $\gamma = \gamma_{\text{opt}}$. Again the minimum RMS error can be computed for each of the 20 noise realizations and the mean value of these errors will be denoted by \mathcal{E}_a .

Table 1. Results of recoverability tests in FFT inversion scheme. Average percent errors in restoring m and a according to the different models chosen for 3% data errors (see text).

	a_1	a_2	a_3
m_1	$\begin{cases} \mathcal{E}_a = 9.5\% \\ \mathcal{E}_m = 6.6\% \end{cases}$	$\begin{cases} \mathcal{E}_a = 35.6\% \\ \mathcal{E}_m = 6.6\% \end{cases}$	$\begin{cases} \mathcal{E}_a = 42.3\% \\ \mathcal{E}_m = 6.6\% \end{cases}$
m_2	$\begin{cases} \mathcal{E}_a = 5.3\% \\ \mathcal{E}_m = 6.8\% \end{cases}$	$\begin{cases} \mathcal{E}_a = 6.3\% \\ \mathcal{E}_m = 6.3\% \end{cases}$	$\begin{cases} \mathcal{E}_a = 14.6\% \\ \mathcal{E}_m = 6.8\% \end{cases}$
m_3	$\begin{cases} \mathcal{E}_a = 9.0\% \\ \mathcal{E}_m = 10.5\% \end{cases}$	$\begin{cases} \mathcal{E}_a = 9.5\% \\ \mathcal{E}_m = 10.3\% \end{cases}$	$\begin{cases} \mathcal{E}_a = 13.7\% \\ \mathcal{E}_m = 9.8\% \end{cases}$

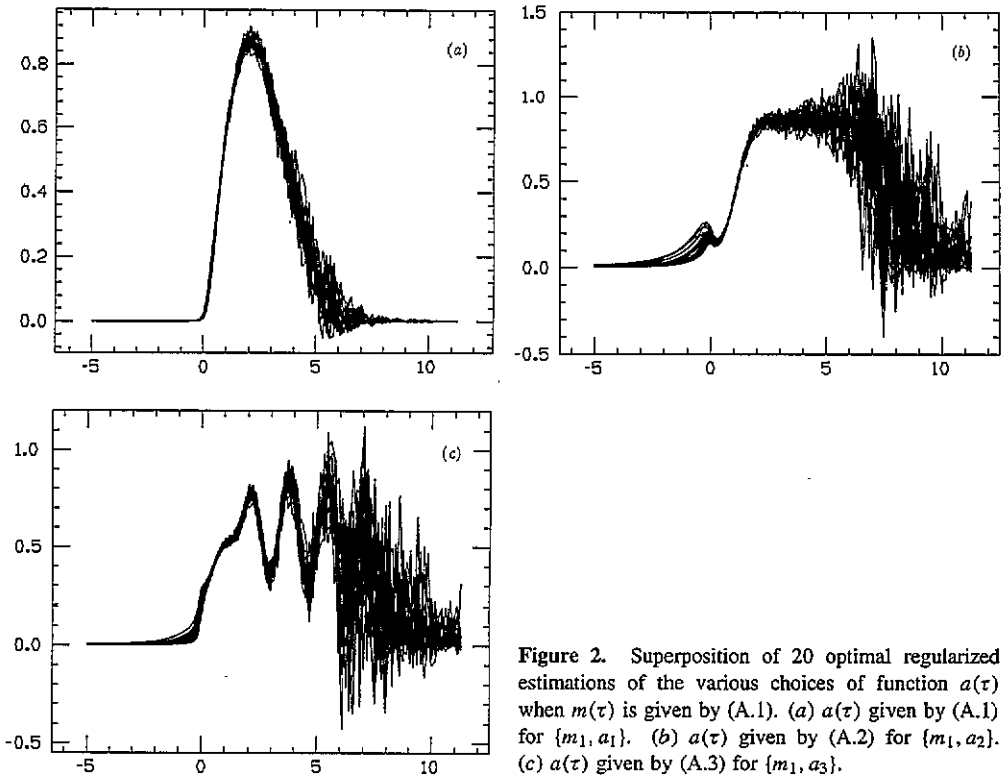


Figure 2. Superposition of 20 optimal regularized estimations of the various choices of function $a(\tau)$ when $m(\tau)$ is given by (A.1). (a) $a(\tau)$ given by (A.1) for $\{m_1, a_1\}$. (b) $a(\tau)$ given by (A.2) for $\{m_1, a_2\}$. (c) $a(\tau)$ given by (A.3) for $\{m_1, a_3\}$.

The values of \mathcal{E}_m and \mathcal{E}_a , expressed as % errors, are shown in table 1 for all pairs $\{m_j, a_k\}$. The restoration errors are, in general, larger than the error in the data. However, the restoration error \mathcal{E}_a is especially large in the case of the pairs $\{m_1, a_2\}$ and $\{m_1, a_3\}$. The reason for this is that, precisely in these cases, the function $a(\tau)$ is large in a time interval where $m(\tau)$ is small.

In figure 2 we show the effect of superimposing 20 restorations of the functions $a(\tau)$ in the cases $\{m_1, a_1\}$, $\{m_1, a_2\}$ and $\{m_1, a_3\}$. The nearly black regions obtained define the band of oscillation, where any regularized restoration can wiggle as a consequence of noise. In fact, for each value of τ , the width of this region defines a sort of error bar for the reconstruction. In particular, one finds, in agreement with the previous remark, that where the values of $m(\tau)$ are smaller the error in the restoration of $a(\tau)$ is larger. In particular, figure 2(a), which corresponds to case $\{m_1, a_1\}$ (i.e. $a = m$), is practically equivalent to the superposition of all the restorations of function $m(\tau)$ that have been done in the case of pairs corresponding to the first row of table 1 and gives an idea of the accuracy of the restoration of the function $m(\tau)$ (compare with figure 1(a)).

As clearly appears from figures 2(b) and 2(c), the minimization of $\mathcal{E}_a(\gamma)$ provides a value of γ which is too small, as a consequence one finds a large numerical instability in the time interval where $m(\tau)$ is small. A related effect is that one finds non-zero values of $a(\tau)$ in the region $\tau < 0$, i.e. causality is violated in the restoration process. For these reasons we have investigated other criteria for the choice of γ . As an example we give the results obtained by minimizing the following discretized version of a weighted Sobolev norm

$$\|a - a_\gamma\|_S = \left(\sum_i \{w_0(\tau_i)|a(\tau_i) - a_\gamma(\tau_i)|^2 + w_1(\tau_i)|a'(\tau_i) - a'_\gamma(\tau_i)|^2\} \right)^{1/2} \quad (2.18)$$

where $a'(\tau)$ and $a'_\gamma(\tau)$ are the first derivatives of $a(\tau)$ and $a_\gamma(\tau)$, respectively, and the weights $w_0(\tau)$ and $w_1(\tau)$ are defined in terms of $m(\tau)$ as

$$w_0(\tau) = \frac{m^2(\tau)}{m^2(\tau) + \mu \overline{m^2}}, \quad w_1(\tau) = \frac{\mu \overline{m^2}}{m^2(\tau) + \mu \overline{m^2}} \quad (2.19)$$

$$\overline{m^2} = \frac{1}{16} \int_{-5}^{11} m^2(\tau) d\tau \cong \frac{1}{N'} \sum_{i=1}^{N'} m^2(\tau_i). \quad (2.20)$$

Here N' is the number of sampling points belonging to the interval $[-5, 11]$ and μ is a parameter which controls the relative weight of the two terms in (2.18) ($\mu = 0$ corresponds to the norm (2.17) while $\mu = \infty$ corresponds to the same norm for $a'(\tau)$).

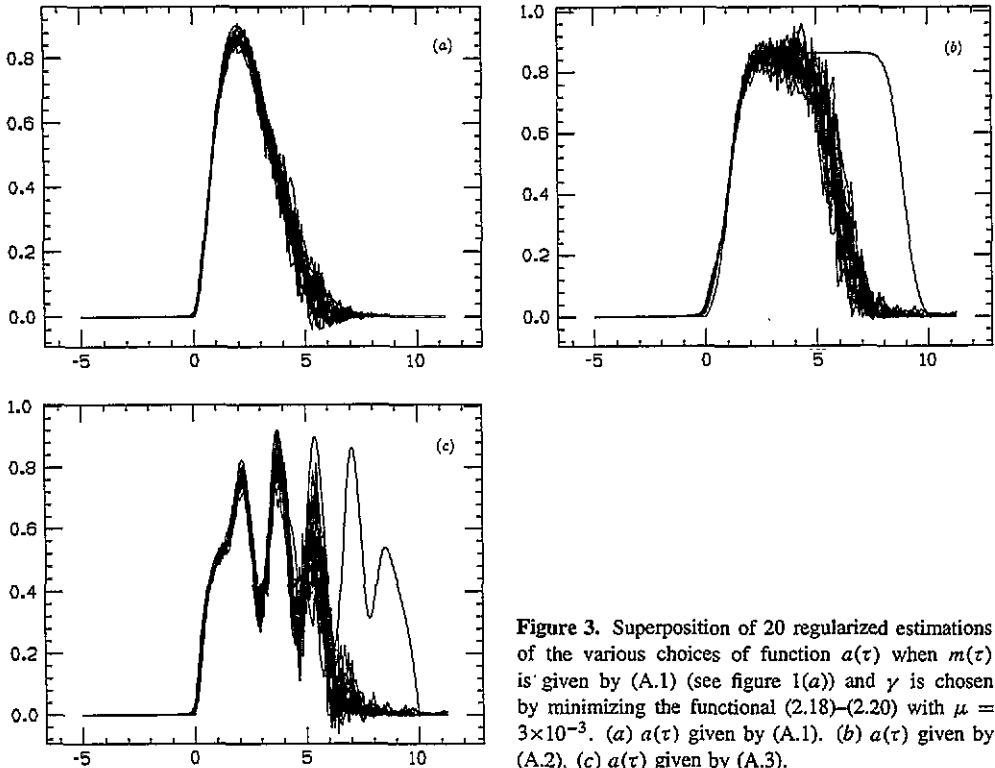


Figure 3. Superposition of 20 regularized estimations of the various choices of function $a(\tau)$ when $m(\tau)$ is given by (A.1) (see figure 1(a)) and γ is chosen by minimizing the functional (2.18)–(2.20) with $\mu = 3 \times 10^{-3}$. (a) $a(\tau)$ given by (A.1). (b) $a(\tau)$ given by (A.2). (c) $a(\tau)$ given by (A.3).

In figure 3 we show the restorations obtained in the case $\mu = 3 \times 10^{-3}$. We find that now the restorations of $a(\tau)$ are much more stable and satisfy the causality condition. Moreover, these restorations provide small values of $a(\tau)$ in the time interval where $m(\tau)$ is small, in agreement with the fact that the data contain poor information about the values of $a(\tau)$ in this interval.

3. The case of discrete data: formulation in a Sobolev space

The results of the previous section are promising, but require a distribution of data points which is never obtained in practice. A more realistic formulation is the following one. We assume that the observation interval is $[0, T]$ and that the episodic outburst is localized in that interval. Moreover, we assume that N values of $F(\tau)$ are measured at times τ_i in $[0, T]$, so that the integral equation (2.7) is replaced by

$$F_i = F(\tau_i) = \int_0^T K_i(\tau) f(\tau) d\tau \quad i = 1, 2, \dots, N \quad (3.1)$$

where the functions $K_i(\tau)$ are given by

$$K_i(\tau) = \begin{cases} \frac{\sqrt{(\tau_i - \tau)(\tau_i - \tau + 2)}}{(\tau_i - \tau + 1)^3} & 0 \leq \tau \leq \tau_i \\ 0 & \tau_i < \tau \leq T. \end{cases} \quad (3.2)$$

Analogously, we assume that \bar{N} values of $G(\tau)$ are measured at times $\bar{\tau}_k$ in $[0, T]$, so that the integral equation (2.8) is replaced by

$$G_k = G(\bar{\tau}_k) = \int_0^T H_k(\tau) g(\tau) d\tau \quad k = 1, 2, \dots, \bar{N} \quad (3.3)$$

where the functions $H_k(\tau)$ are given by

$$H_k(\tau) = \begin{cases} \frac{1}{(\bar{\tau}_k - \tau + 1)^2} & 0 \leq \tau \leq \bar{\tau}_k \\ 0 & \bar{\tau}_k < \tau \leq T. \end{cases} \quad (3.4)$$

Therefore the problem is to find functions $f(\tau)$ and $g(\tau)$, given their scalar products with the functions $K_i(\tau)$ and $H_k(\tau)$, respectively. In $L^2(0, T)$ the solutions of these problems are not unique, so that one usually looks for minimal norm solutions $f^+(\tau)$ and $g^+(\tau)$. In the case of the minimization of the L^2 -norm, $f^+(\tau)$ is a linear combination of the functions $K_i(\tau)$, while $g^+(\tau)$ is a linear combination of the functions $H_k(\tau)$ [15]. Therefore the functions $m(\tau)$ and $a(\tau)$ are linear combinations both of $K_i(\tau)$ and of $H_k(\tau)$.

These functions exhibit some kind of discontinuity at the points τ_i and $\bar{\tau}_k$, respectively. As far as the functions $K_i(\tau)$ are concerned, the discontinuity is in the first derivatives (at $\tau = \tau_i$) while in the case of the functions $H_k(\tau)$ the functions themselves are discontinuous (at $\tau = \bar{\tau}_k$). Therefore the functions $m(\tau)$ and $a(\tau)$ have discontinuities at all the observation points τ_i and $\bar{\tau}_k$. Since these discontinuities are, in general, unphysical, we must look for a different approach.

A way of obtaining solutions without discontinuities is to look for minimal norm solutions in a space of differentiable functions (Sobolev space) [16]. Since the problems (3.1) and (3.3) are independent, we simply show how our method applies to (3.1). Its extension to (3.3) requires only obvious changes.

Since we assume that the episodic mass loss is not only continuous, but also localized in the interval $[0, T]$, we can assume that $f(0) = f(T) = 0$. Then the broadest space of differentiable functions satisfying these conditions is

$$X = \{f \in L^2(0, T) | f' \in L^2(0, T); f(0) = f(T) = 0\}. \quad (3.5)$$

This is a Hilbert space (it is an example of Sobolev space), complete with respect to the norm

$$\|f\|_X = \left(\int_0^T |f'(\tau)|^2 d\tau \right)^{1/2}. \quad (3.6)$$

Now, in order to formulate the problem (3.1) as a problem in X , we must write the L^2 scalar products, which appear in (3.1), as scalar products in X . For this purpose we must find functions $\psi_i \in X$ such that, for any function $f \in X$, we have

$$\int_0^T f(\tau) K_i(\tau) d\tau = \int_0^T f'(\tau) \psi_i'(\tau) d\tau. \quad (3.7)$$

By means of a partial integration in the right-hand integral, since X is dense in $L^2(0, T)$, one finds that each $\psi_i(\tau)$ is the solution of the boundary value problem

$$\psi_i''(\tau) = -K_i(\tau) \quad \psi_i(0) = \psi_i(T) = 0 \quad (3.8)$$

(the boundary conditions follow from the requirement that $\psi_i \in X$). This problem is solved in appendix B, where it is shown that

$$\psi_i(\tau) = \tau \alpha_i(\tau) + \beta_i(\tau) - \frac{\tau}{T} \beta_i(\tau_i) \quad (3.9)$$

and expressions are given for the functions $\alpha_i(\tau)$ and $\beta_i(\tau)$. In the same appendix we also solve the analogous differential problem related to the functions $H_k(\tau)$.

Taking (3.7) into account, the problem (3.1) can now be written as

$$F_i = (f, \psi_i)_X \quad i = 1, 2, \dots, N \quad (3.10)$$

and the minimal norm solution is the function $f(\tau)$ satisfying these conditions and such that

$$\|f\|_X = \text{minimum}. \quad (3.11)$$

This minimal norm solution is a linear combination of the functions $\psi_i(\tau)$ and therefore it is differentiable in $[0, T]$ and zero at the boundary points. Such a solution, however, is numerically unstable and consequently one must look for regularized estimates. These can be obtained by means of a singular value decomposition (SVD) of the problem.

As an example, we consider now uniformly spaced data. In such a case it is convenient to introduce the following norm in the N -dimensional data space Y

$$\|F\|_Y = \left(\frac{T}{N} \sum_{i=1}^N |F_i|^2 \right)^{1/2} \quad (3.12)$$

the factor T/N being introduced in order to approximate the L^2 -norm of $F(\tau)$. Moreover, we define a linear operator $L : X \rightarrow Y$ by

$$(Lf)_i = (f, \psi_i)_X \quad i = 1, 2, \dots, N. \quad (3.13)$$

This operator has a singular system, defined by

$$Lv_k = \sigma_k u_k \quad L^* u_k = \sigma_k v_k \quad k = 1, 2, \dots, N \quad (3.14)$$

where $L^* : Y \rightarrow X$ is the adjoint operator. Moreover, it can be shown that [15]

$$L \cdot L^* = G^T \cdot W \quad (3.15)$$

where G^T is the transpose of the Gram matrix G given by

$$G_{ij} = (\psi_i, \psi_j)_X \quad (3.16)$$

and W is the identity matrix multiplied by T/N .

Then the singular values σ_k of the operator L are the square roots of the eigenvalues of the matrix $L \cdot L^*$, the singular vectors u_k in data space are the eigenvectors of $L \cdot L^*$, while the singular functions $v_k(\tau)$ in Sobolev space X can be obtained from

$$v_k(\tau) = \frac{1}{\sigma_k} (L^* u_k)(\tau) \quad (3.17)$$

and are given by

$$v_k(\tau) = \frac{1}{\sigma_k} \frac{T}{N} \sum_{i=1}^N (u_k)_i \psi_i(\tau). \quad (3.18)$$

In our problem numerical computations of the singular system of L are simplified by the fact that the functions ψ_i can be computed analytically and also that matrix elements G_{ij} given by (3.16) can be put in closed form in the case of the functions $H_k(\tau)$. Details of the computation of G_{ij} are given in appendix C.

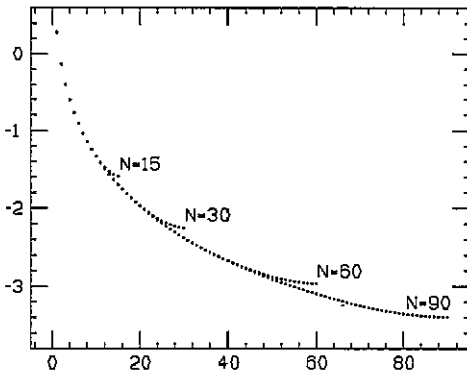


Figure 4. Singular value spectrum of operator L defined by (3.13) with $N = 15, 30, 60$ and 90 . The ordinate is the base 10 logarithm of the eigenvalues.

We present numerical results only in the case of the kernel functions $K_i(\tau)$, since those obtained in the case of the functions $H_i(\tau)$ are quite similar. The singular value spectrum of the operator L is shown in figure 4 where the base 10 logarithm of σ_k is plotted against k , for $N = 15, 30, 60$ and 90 . The convergence of the spectrum when $N \rightarrow \infty$ is clearly illustrated by this figure. It is also clear that the ill-conditioning of the problem increases as N increases. The condition number $\text{Cond}(L) = \sigma_1/\sigma_N$ [15], which gives an estimate of the ill-conditioning of the problem, varies from 75.6 when $N = 15$ up to 4700 when $N = 90$.

In figure 5 we plot the first six singular functions $v_k(\tau)$ for $N = 30$. We notice that $v_k(\tau)$ has exactly $k - 1$ zeros inside the interval $[0, T]$ and therefore the number of oscillations of $v_k(\tau)$ increases as k increases.

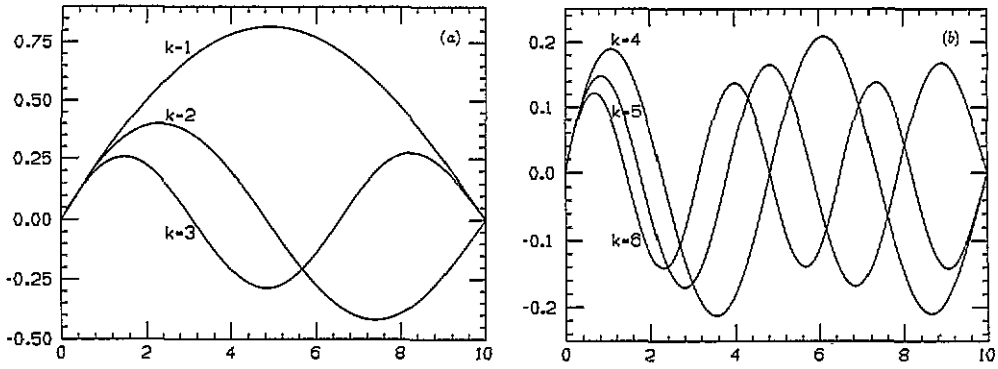


Figure 5. Singular functions of operator L defined by (3.13) with $N = 30$. (a) $k = 1, 2$ and 3 . (b) $k = 4, 5$ and 6 .

4. Uniformly spaced data: inversion in a Sobolev space

The solution of problem (3.10) having minimal norm in X is given by [15]

$$f^+(\tau) = \sum_{k=1}^N \frac{1}{\sigma_k} (F, u_k) \gamma v_k(\tau). \tag{4.1}$$

This solution, however, is ill-conditioned as is shown by the numerical results on the singular value spectrum of L . Therefore one can use a regularized version of (4.1), as given by [14, 15]

$$f_\alpha(\tau) = \sum_{k=1}^N \frac{\sigma_k}{\sigma_k^2 + \alpha} (F, u_k) \gamma v_k(\tau). \tag{4.2}$$

We notice that if we use the singular system computed in section 3, then this function is the function minimizing the functional

$$\Phi_\alpha[f] = \frac{T}{N} \sum_{i=1}^N |(Lf)_i - \tilde{F}_i|^2 + \alpha \int_0^T |f'(\tau)|^2 d\tau \tag{4.3}$$

with the additional boundary conditions

$$f(0) = f(T) = 0. \tag{4.4}$$

Similar remarks apply to the case of the function $g(\tau)$. The singular system appropriate to the restoration of this function has also been computed using the results of appendices B and C. The regularized solution will be denoted by $g_\beta(\tau)$.

Just as we did in the case of Fourier transform inversion, we have tested the previous inversion method employing the same test functions used in section 2 (see (A.1)–(A.3)). For each $\{m_j, a_k\}$ pair we have assumed, for simplicity, that both $F(\tau)$ and $G(\tau)$ are given at the same points τ_i . Moreover, we have taken 30 equidistant points in the interval $[0, 10]$, a number of points much smaller (and in a smaller interval) than that considered in section 2. For each point, $\tilde{F}(\tau_i)$ and $\tilde{G}(\tau_i)$ have been computed from (3.1) and (3.3), respectively,

by means of a numerical integration routine. Then 3% Gaussian noise was added to these values (see (2.14) and (2.15)) to generate 20 realizations of noisy data for each $\{m_j, a_k\}$ pair.

Regularized solutions $f_\alpha(\tau)$ and $g_\beta(\tau)$ can be computed using (4.2) for $f_\alpha(\tau)$ and a similar equation for $g_\beta(\tau)$. Moreover, the functions $m(\tau)$ and $a(\tau)$ can be obtained from (2.9) and (2.13), respectively. The choice of the optimum values of the regularization parameters was performed by minimizing the relative RMS errors introduced in section 2. The sum in the RHS of (2.17) was extended to a set of 401 points uniformly spaced in the interval $[0, 10]$. The results of our tests are presented in table 2 in terms of average percent errors in the estimation of $m(\tau)$ and $a(\tau)$ and can be directly compared with those shown in table 1 concerning Fourier inversion tests. The results are better than those found using the Fourier method, despite the use of much fewer points. This effect is due to the extra information implied by the assumption that the solution has a bounded support (the interval $[0, T]$), is differentiable and satisfies the boundary conditions (4.4). Also in this scheme, however, the recoverability of $a(\tau)$ is uncertain when the effective support of $m(\tau)$ is smaller than the effective support of $a(\tau)$, as occurs in the pairs $\{m_1, a_2\}$ and $\{m_1, a_3\}$.

Table 2. Results of recoverability tests in the Sobolev inversion scheme. Average percent errors in restoring m and a according to the different models chosen for 3% data errors (see text).

	a_1	a_2	a_3
m_1	$\begin{cases} \mathcal{E}_a = 7.5\% \\ \mathcal{E}_m = 3.2\% \end{cases}$	$\begin{cases} \mathcal{E}_a = 33.4\% \\ \mathcal{E}_m = 3.3\% \end{cases}$	$\begin{cases} \mathcal{E}_a = 39.6\% \\ \mathcal{E}_m = 4.9\% \end{cases}$
m_2	$\begin{cases} \mathcal{E}_a = 4.5\% \\ \mathcal{E}_m = 3.8\% \end{cases}$	$\begin{cases} \mathcal{E}_a = 5.3\% \\ \mathcal{E}_m = 3.7\% \end{cases}$	$\begin{cases} \mathcal{E}_a = 12.8\% \\ \mathcal{E}_m = 5.5\% \end{cases}$
m_3	$\begin{cases} \mathcal{E}_a = 7.3\% \\ \mathcal{E}_m = 7.1\% \end{cases}$	$\begin{cases} \mathcal{E}_a = 7.8\% \\ \mathcal{E}_m = 7.4\% \end{cases}$	$\begin{cases} \mathcal{E}_a = 11.8\% \\ \mathcal{E}_m = 6.8\% \end{cases}$

We do not give pictures of the restored functions because these are rather similar to those obtained with the Fourier method. Also, in the present case the criterion of minimizing the relative RMS error in the restoration of $a(\tau)$ provides a value of γ which is too small. If one uses larger values of γ as, for instance, those provided by the criterion proposed in section 2 and based on the minimization of a weighted Sobolev norm, then one finds features similar to those discussed in section 2.

However, the method of determining the optimal values of the regularization parameters by minimization of the RMS error in the restoration of the functions $f(\tau)$, $g(\tau)$ and $a(\tau)$ can be used only in the case of simulated data. In the case of real data such a procedure obviously does not work.

In the literature many methods have been proposed for determining the regularization parameter when one has to deal with real data. The effectiveness of each one of them is still controversial, so we have tried to test the reliability of eight of them in our particular problem. From the review by Davies [17] we have chosen seven methods and have taken one other from [18]:

- (1) Discrepancy Principle (DIS)
- (2) Turchin's Method (TUR)
- (3) Generalized Cross-Validation (GCV)
- (4) Quasioptimal Method of Tikhonov and Glasko (QUA)
- (5) Leonov's Ratio Criterion (LEO)

- (6) L-Curve Criterion (LCU)
- (7) Maximum Likelihood (MAX)
- (8) Unbiased Risk Method (UNB).

Our purpose is to compare the values provided by these methods with the optimum one obtained by minimizing the RMS restoration error.

For simplicity we have considered the problem of recovering the function $f(\tau)$ by taking $f(\tau) = h_1(\tau/10)$ (see (A.1)). Therefore we have only investigated the problem of determining the regularization parameter α .

We have computed the integral in (3.1) for 30 values of τ uniformly spaced in the interval $[0,10]$. We have generated 20 sets of data by adding 3% Gaussian noise to these 30 values according to the scheme of (2.14). Then we have applied each one of these eight methods to each of the 20 data sets and compared the values of the α parameter they provide with the optimum one (OPT) obtained by minimizing the RMS restoration error. In table 3 the results of this test are shown. In particular, it can be noticed that methods QUA, LEO, DIS and TUR usually give an overregularized estimate, whereas the others tend to give an underregularized one. It is worthwhile remarking that the GCV method sometimes fails because its curve has no minimum. Then one should, as suggested by some authors, search for the point where the curve suddenly starts to rise. In the example we studied we found two cases of data sets whose GCV curve was without a minimum, but in these cases the point where the curve rises provides a reasonable value of α .

Table 3. The eight methods considered for determining the regularization parameter α compared with the minimum RMS error method (OPT). Each row shows the method considered, the minimum value for α in the set of the 20 values obtained, the maximum value for α , the average value for α , the standard deviation for α and, last, the average relative RMS error in the restoration.

	α				error average
	min	max	average	stand. dev.	
OPT	1.19×10^{-3}	5.97×10^{-3}	2.72×10^{-3}	1.24×10^{-3}	3.8%
DIS	2.85×10^{-3}	8.22×10^{-3}	5.48×10^{-3}	1.46×10^{-3}	4.3%
TUR	2.79×10^{-3}	8.13×10^{-3}	5.39×10^{-3}	1.46×10^{-3}	4.3%
GCV	6.56×10^{-5}	2.92×10^{-3}	1.37×10^{-3}	8.75×10^{-4}	4.9%
QUA	1.80×10^{-3}	1.88×10^{-2}	1.25×10^{-2}	4.54×10^{-3}	6.0%
LEO	3.54×10^{-3}	1.75×10^{-2}	1.13×10^{-2}	3.46×10^{-3}	5.7%
LCU	3.91×10^{-4}	1.74×10^{-3}	8.80×10^{-4}	3.78×10^{-4}	4.7%
MAX	2.02×10^{-5}	3.70×10^{-4}	1.81×10^{-4}	1.08×10^{-4}	8.1%
UNB	8.54×10^{-4}	2.14×10^{-3}	1.44×10^{-3}	3.71×10^{-4}	4.2%

5. Conclusions

We have established and tested a robust and flexible algorithm for joint derivation of episodic stellar mass loss rate $m(\tau)$ and shape $a(\tau)$ functions from overlapping data on stellar wind polarization and absorption line strength. Our formulation in terms of singular value decomposition (SVD) is a major improvement on the Brown and Wood [13] FFT description in reducing the number of support points required and removing the restriction to uniformly spaced (or interpolated) data. Indeed the two data sets need only span the same interval, but need not involve simultaneous points.

The presence of discontinuities in the kernel functions makes a (zero-order) regularized SVD solution with L^2 -norm minimization unsuitable. However we have been able to obtain an SVD solution in a Sobolev space of differentiable functions. A (first-order) regularized solution in this space yields reliable results, in the presence of realistic data noise, for a wide variety of combinations of simulated $m(\tau)$ and $a(\tau)$ functions. The only notable exceptions reveal a problem in deriving the shape $a(\tau)$ when the mass loss rate $m(\tau)$ is small.

Thus we have obtained not only a more efficient and versatile method than Wood and Brown [13], but also applied it jointly to derivations of general $m(\tau)$ and $a(\tau)$ whereas their illustration was solely in the case $a(\tau) = \text{constant}$. Our algorithm will be applied to real data, and the effects of sparse data sampling investigated, in a subsequent paper.

Acknowledgments

The financial support of grants from the UK Science and Engineering Research Council, from NATO and from Italian M.U.R.S.T. and I.N.F.M. is gratefully acknowledged.

Appendix A

Here we present the formulae giving the three functions h_i ($i = 1, 2, 3$) used in the recoverability tests of m and a profiles (sections 2 and 4). These are functions of τ with support on the interval $[0, 10]$, but for simplicity we define them as functions of the variable $y = \tau/10$ on $[0, 1]$.

The first one, $h_1(y)$, is given by

$$h_1(y) = 150y^2(1 - y)^4 \exp(-5y) \quad (\text{A.1})$$

and is shown in figure 1(a).

The second one, $h_2(y)$, has a plateau behaviour as shown in figure 1(b) and is generated by the expression

$$h_2(y) = \frac{0.05}{0.055 + (2y - 1)^{12}} - 0.0474. \quad (\text{A.2})$$

The third one, $h_3(y)$, has an oscillating behaviour as shown in figure 1(c) and is given by the expression

$$h_3(y) = 0.65b(y) + 0.33c^2(y) \sin(12\pi y) \quad (\text{A.3})$$

where the functions $b(y)$ and $c(y)$ are defined by

$$b(y) = [1 - (2y - 1)^8] \exp(-0.25y)$$

and

$$c(y) = \frac{0.05}{0.05 + (2y - 1)^8}.$$

Appendix B

The solution of the boundary value problem (3.8) can be written as

$$\psi_i(\tau) = \tau\alpha_i(\tau) + \beta_i(\tau) - \frac{\tau}{T}\beta_i(\tau_i) \quad (\text{B.1})$$

where

$$\alpha_i(\tau) = \int_{\tau}^T K_i(\tau') d\tau' \quad (\text{B.2})$$

and

$$\beta_i(\tau) = \int_0^{\tau} \tau' K_i(\tau') d\tau'. \quad (\text{B.3})$$

Explicit expressions can be given by defining the auxiliary functions

$$\phi_2(x) = -\frac{\sqrt{x(x+2)}}{x+1} + \ln[x+1+\sqrt{x(x+2)}] \quad [\phi_2(0) = 0] \quad (\text{B.4})$$

and

$$\phi_3(x) = \frac{1}{2} \left[\tan^{-1}(\sqrt{x(x+2)}) - \frac{\sqrt{x(x+2)}}{(x+1)^2} \right] \quad [\phi_3(0) = 0]. \quad (\text{B.5})$$

With these definitions we have

$$\alpha_i(\tau) = \begin{cases} \phi_3(\tau_i - \tau) & 0 \leq \tau \leq \tau_i \\ 0 & \tau_i \leq \tau \leq T \end{cases} \quad (\text{B.6})$$

$$\beta_i(\tau) = \begin{cases} (\tau_i + 1)[\phi_3(\tau_i) - \phi_3(\tau_i - \tau)] - \phi_2(\tau_i) + \phi_2(\tau_i - \tau) & 0 \leq \tau \leq \tau_i \\ (\tau_i + 1)\phi_3(\tau_i) - \phi_2(\tau_i) & \tau_i \leq \tau \leq T. \end{cases} \quad (\text{B.7})$$

$$\beta_i(\tau) = \begin{cases} (\tau_i + 1)[\phi_3(\tau_i) - \phi_3(\tau_i - \tau)] - \phi_2(\tau_i) + \phi_2(\tau_i - \tau) & 0 \leq \tau \leq \tau_i \\ (\tau_i + 1)\phi_3(\tau_i) - \phi_2(\tau_i) & \tau_i \leq \tau \leq T. \end{cases} \quad (\text{B.8})$$

In the case of the kernels $H_k(\tau)$ given by (3.4), we must introduce functions $\bar{\psi}_k(\tau)$, analogous to the functions $\psi_i(\tau)$ and defined as the solutions of the boundary value problems

$$\bar{\psi}_k''(\tau) = -H_k(\tau) \quad \bar{\psi}_k(0) = \bar{\psi}_k(T) = 0. \quad (\text{B.9})$$

For these functions one also gets expressions analogous to (B.1)–(B.3), with $K_i(\tau')$ replaced by $H_k(\tau')$. By denoting by $\bar{\alpha}_k(\tau)$ and $\bar{\beta}_k(\tau)$ the functions corresponding in this case to $\alpha_i(\tau)$ and $\beta_i(\tau)$ of the former case, we obtain

$$\bar{\alpha}_k(\tau) = \begin{cases} \frac{\bar{\tau}_k - \tau}{1 + \bar{\tau}_k - \tau} & 0 \leq \tau \leq \bar{\tau}_k \\ 0 & \bar{\tau}_k \leq \tau \leq T \end{cases} \quad (\text{B.10})$$

$$\bar{\beta}_k(\tau) = \begin{cases} \frac{\tau}{1 + \bar{\tau}_k - \tau} - \ln\left(\frac{1 + \bar{\tau}_k}{1 + \bar{\tau}_k - \tau}\right) & 0 \leq \tau \leq \bar{\tau}_k \\ \bar{\beta}_k(\bar{\tau}_k) = \bar{\tau}_k - \ln(1 + \bar{\tau}_k) & \bar{\tau}_k \leq \tau \leq T. \end{cases} \quad (\text{B.11})$$

$$\bar{\beta}_k(\tau) = \begin{cases} \frac{\tau}{1 + \bar{\tau}_k - \tau} - \ln\left(\frac{1 + \bar{\tau}_k}{1 + \bar{\tau}_k - \tau}\right) & 0 \leq \tau \leq \bar{\tau}_k \\ \bar{\beta}_k(\bar{\tau}_k) = \bar{\tau}_k - \ln(1 + \bar{\tau}_k) & \bar{\tau}_k \leq \tau \leq T. \end{cases} \quad (\text{B.12})$$

Appendix C

According to the definition of the scalar product in X , the elements of the Gram matrix of problem (3.1) are given by

$$G_{ij} = \int_0^T \psi'_i(\tau)\psi'_j(\tau) d\tau. \quad (C.1)$$

Using (B.1)–(B.3) it can easily be proved that

$$\psi'_i(\tau) = \alpha_i(\tau) - \frac{\beta_i(\tau_i)}{T}. \quad (C.2)$$

Then by substitution of (C.2) into (C.1) we get

$$G_{ij} = \int_0^T \alpha_i(\tau)\alpha_j(\tau) d\tau - \frac{1}{T} \int_0^T [\beta_i(\tau_i)\alpha_j(\tau) + \beta_j(\tau_j)\alpha_i(\tau)] d\tau + \frac{1}{T} \beta_i(\tau_i)\beta_j(\tau_j). \quad (C.3)$$

Moreover, from (C.2) and from boundary conditions contained in (3.8) it can easily be shown that

$$\int_0^T \alpha_i(\tau) d\tau = \beta_i(\tau_i). \quad (C.4)$$

So, taking (B.6) into account, one can reduce (C.1) for $\tau_i \leq \tau_j$ to

$$G_{ij} = \int_0^{\tau_i} \alpha_i(\tau)\alpha_j(\tau) d\tau - \frac{1}{T} \beta_i(\tau_i)\beta_j(\tau_j). \quad (C.5)$$

As the Gram matrix is symmetric, the terms G_{ij} with $\tau_i > \tau_j$ can also be derived from (C.5) simply by computing G_{ji} .

Equation (C.5) was really used to compute the Gram matrix by evaluating numerically the integral which appears in this equation. As concerns problem (3.3) in X , the elements of its Gram matrix are given by

$$\bar{G}_{i,j} = \int_0^{\bar{\tau}_i} \bar{\psi}'_i(\tau)\bar{\psi}'_j(\tau) d\tau \quad (C.6)$$

and they can also be reduced to the form (C.5). But now the integrals can be computed analytically as follows

$$\begin{aligned} & \int_0^{\bar{\tau}_i} \bar{\alpha}_i(\tau)\bar{\alpha}_j(\tau) d\tau \\ &= \bar{\tau}_i + \ln \left[\frac{\bar{\tau}_j - \bar{\tau}_i + 1}{(\bar{\tau}_i + 1)(\bar{\tau}_j + 1)} \right] \\ & \quad + \frac{1}{\bar{\tau}_j - \bar{\tau}_i} \ln \left[\frac{(\bar{\tau}_i + 1)(\bar{\tau}_j - \bar{\tau}_i + 1)}{\bar{\tau}_j + 1} \right] \quad \bar{\tau}_i < \bar{\tau}_j \end{aligned} \quad (C.7)$$

and

$$\int_0^{\bar{\tau}_i} \bar{\alpha}_i^2(\tau) d\tau = \frac{\bar{\tau}_i(\bar{\tau}_i + 2)}{\bar{\tau}_i + 1} - 2 \ln(\bar{\tau}_i + 1) \quad \bar{\tau}_i = \bar{\tau}_j. \quad (C.8)$$

References

- [1] Parker E N 1958 Dynamics of the interplanetary gas and magnetic fields *Astrophys. J.* **128** 664–76
- [2] Bierman L 1951 Kometenschweife und solare Korpuskularstrahlung *Z. Astrophys.* **29** 274–86
- [3] Gringauz K I, Bezrukhikh V V, Ozerov V D and Rybchinskii R E 1960 Study of the interplanetary ionized gas, high-energy electrons and corpuscular radiation of the sun employing three electrode charged particle traps on the second Soviet space rocket *Sov. Phys. Dokl.* **5** 361–4
- [4] Hundhausen A J 1973 *Coronal Expansion and Solar Wind* (Berlin: Springer)
- [5] Lamers H J L M 1994 Observational aspects of wind variability *Quebec Workshop on Variability and Instability in Hot Star Winds* ed A J F Moffat, S P Owocki, A Fullerton and N St Louis (Dordrecht: Kluwer) in press
- [6] Cassinelli J P and MacGregor K B 1986 Stellar chromospheres, coronae and winds *Physics of the Sun* ed T E Holzer, D M Mihalas and R K Ulrich, vol 3 (Dordrecht: Reidel) pp 47–124
- [7] Owocki S P 1994 Current status of wind instability simulations *Quebec Workshop on Variability and Instability in Hot Star Winds* ed A J F Moffat, S P Owocki, A Fullerton and N St Louis N (Dordrecht: Kluwer) in press
- [8] Brown J C 1994 Spectropolarimetric modeling of hot star wind structure *Quebec Workshop on Variability and Instability in Hot Star Winds* ed A J F Moffat, S P Owocki, A Fullerton and N St Louis N (Dordrecht: Kluwer) in press
- [9] Brown J C and Wood K H 1994 Analytic inversion of Thomson scattered spectropolarimetric line profiles to yield the velocity structure of rotating or expanding circumstellar disks *Astron. Astrophys.* **290** 634–43
- [10] Wood K H and Brown J C 1994 Parametric inversion of Thomson scattered spectropolarimetric line profiles to yield the velocity structure of rotating or expanding circumstellar disks *Astron. Astrophys.* **285** 220–8
- [11] Brown J C and Henrichs H F 1987 The relation between the visual polarization and UV narrow absorption lines in irregular Be star variations *Astron. Astrophys.* **182** 107–14
- [12] Sonneborn G, Grady C A, Chi-Chao W, Hayes D P, Guinan E F, Barker P K and Henrichs H F 1988 Mass loss in a B2 IIIe star: ω Orionis 1978–84 *Astrophys. J.* **325** 784–94
- [13] Brown J C and Wood K H 1992 Derivation of episodic mass loss functions for hot stars from polarimetric and absorption line data *Astron. Astrophys.* **265** 663–8
- [14] Craig I J D and Brown J C 1986 *Inverse Problems in Astronomy* (Bristol: Adam Hilger)
- [15] Bertero M 1989 Linear inverse and ill-posed problems *Advances in Electronics and Electron Physics* vol 75, ed P W Hawkes (New York: Academic) pp 1–120
- [16] Bardati F, Bertero M, Mongiardo M and Solimini D 1987 Singular system analysis of the inversion of microwave radiometric data: applications to biological temperature retrieval *Inverse Problems* **3** 347–70
- [17] Davies A M 1992 Optimality in regularization *Inverse Problems in Scattering and Imaging* ed M Bertero and E R Pike (Bristol: Adam Hilger) pp 393–410
- [18] Hansen P C 1992 Analysis of discrete ill-posed problems by means of the L-curve *SIAM Rev.* **34** 561–80